Fabrication and *ab initio* study of downscaled graphene nanoelectronic devices

Hiroshi Mizuta[1,2]*, Zakaria Moktadir[1], Stuart A. Boden[1], Nima Kalhor[1], Shuojin Hang[1], Marek E Schmidt[1], Nguyen Tien Cuong[2], Dam Hieu Chi[2], Nobuo Otsuka[2], Muruagnathan Manoharan[2], Yoshishige Tsuchiya[1], Harold Chong[1], Harvey N. Rutt[1] and Darren M. Bagnall[1]
[1]Nano Group, ECS, Faculty of Physical and Applied Sciences, Univ. of Southampton, Highfield, Southampton SO17 1BJ, UK;
[2]School of Materials Science, Japan Advanced Institute of Science and Technology (JAIST), 1-1 Asahi-dai, Nomi, Ishikawa 923-1292, Japan

ABSTRACT

In this paper we first present a new fabrication process of downscaled graphene nanodevices based on direct milling of graphene using an atomic-size helium ion beam. We address the issue of contamination caused by the electron-beam lithography process to pattern the contact metals prior to the ultrafine milling process in the helium ion microscope (HIM). We then present our recent experimental study of the effects of the helium ion exposure on the carrier transport properties. By varying the time of helium ion bombardment onto a bilayer graphene nanoribbon transistor, the change in the transfer characteristics is investigated along with underlying carrier scattering mechanisms. Finally we study the effects of various single defects introduced into extremely-scaled armchair graphene nanoribbons on the carrier transport properties using *ab initio* simulation.

Keywords: Graphene, helium ion microscope, nanofabrication, quantum dot, nanoribbon, point defect, disorder, *ab initio* simulation

1. INTRODUCTION

Graphene is attracting massive worldwide interest for its potential to be the foundation of a new generation of nanoscale electronic/photonic/spintronic devices [1, 2]. This is owing to its remarkable material properties that include very high carrier mobilities [3] and large current carrying capabilities. High intrinsic cutoff frequencies up to 300 GHz have already been achieved with a self-aligned gate graphene transistor [4]. The carrier mobility in graphene is weakly dependent on temperature which implies the mobility is only limited by impurities and/or defects and hence can be further increased by improving material and device fabrication processes. Graphene is a low noise material meaning it is highly sensitive to the environment which makes it an excellent candidate for extreme sensing applications like a single bio/chemical molecular sensor [5]. The electrons in graphene are not much affected by electron – electron interaction and have a long mean free path [6]. In addition, spin-orbit coupling and hyperfine interactions with carbon nuclei are both small in graphene, and a very long spin relaxation length has been demonstrated [7]. All these superior transport properties encourage us to downscale graphene devices further to the regime where we can fully exploit the coherent natures of electronic and spin states. However, this requires the development of ultrafine patterning technologies which enables accurate nanoscale fabrication beyond the present electron-beam lithography technique. In this paper, we present our recent attempts of using an atomic-size helium ion beam to pattern graphene nanostructures directly and also investigate damage caused by helium ion bombardment onto graphene nanoribbons (GNRs) along with preliminary analysis of the impacts of various single defects introduced in the GNRs by using atomistic simulation.

2. FABRICATION OF DOWNSCALED GRAPHENE DEVICES USING HELIUM ION BEAM

Currently, the most established graphene device fabrication technique uses electron-beam (EB) lithography to pattern resist deposited on top of the graphene, followed by oxygen plasma etching [8, 9]. Figure 1(a) shows double quantum dots (QDs) with five side gates patterned by EB lithography with thin PMMA 495K (~42nm) EB resist and etched using

*hm2@ecs.soton.ac.uk, mizuta@jaist.ac.jp; phone +44(0)2380 592852, +81(0)761 51 1571; www.ecs.soton.ac.uk/people/hm2

O_2 /Ar (1:4) plasma generated in an RIE system. Here the QD size is ~40×70nm^2 and the width of constrictions is less than 30nm. The separation between the side gates and QDs is ~80nm. However, parameters such as proximity effect, thickness uniformity of resist layer, and manual development of samples after e-beam lithography have limited the resolution of this method. Recently, a new patterning technique based on direct milling of graphene using a focused beam of helium ions generated in a helium ion microscope (HIM) has emerged [10, 11]. Helium ion microscopy (HIM) is a new surface imaging technique that involves scanning a focused beam of helium ions across a surface to generate an image from the resulting secondary electron (SE) emission, in a similar way to scanning electron microscopy (SEM) [12, 13]. An atomically sharp and extremely bright source, combined with the larger momentum (and so shorter de Broglie wavelength) of helium ions compared to electrons, enables a sub-nanometer probe size at the sample surface and so high resolution imaging. Researchers have demonstrated that the tool can also be used to selectively sputter graphene to create intricate nanoscale designs, offering the potential of resist-free patterning of graphene on a finer scale compared to other techniques [14, 15].

Patterning of graphene in a HIM involves firstly locating an interested graphene flake on the sample by imaging at a low magnification. The magnification is then increased and control is switched to a pattern generator to scan the beam in the required pattern. It is known that low energy ionic bombardment can cause damage to the graphene lattice [16] so it is important to establish whether HIM imaging to locate a suitable area for patterning can be carried out whilst avoiding damage to the graphene to the extent that the electronic properties are degraded. Figure 1(b) shows a pair of double QDs devices with double side gates directly milled on a pristine exfoliated bilayer graphene. The spacing between QDs and side gates and that between the double QD pair are both less than 10 nm, which is difficult to achieve using the conventional EB lithography technique. This QDs structure was fabricated on a pristine graphene flake for demonstration without electrical contacts, and the further process development we need is obviously to combine EB lithography to fabricate the metal contacts as shown in Fig. 1(c) with the HIM milling to pattern downscaled graphene nanostructures. In this section, we describe our HIM milling fabrication process in detail.

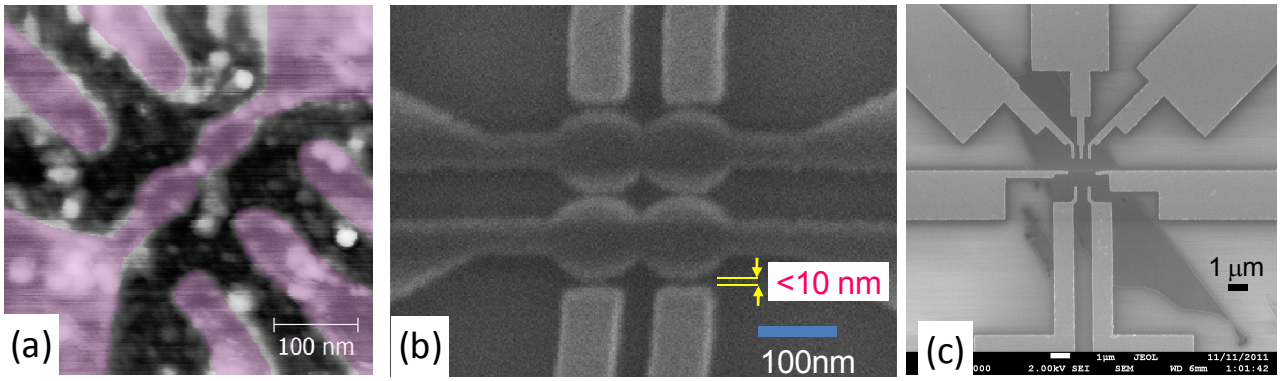

Figure 1 (a) AFM image of a grapheme double QDs with a few side gates patterned on an exfoliated monolayer graphene flake by using electron beam lithography and O_2 plasma RIE. The purple region indicates the graphene flakes while the dark region is SiO_2 substrate, (b) Four QDs patterned on an exfoliated pristine bilayer graphene using He ion beam milling, and (c) Multiple metal contacts fabricated on an exfoliated graphene flake fabricated by EB lithography.

Metal contacts on graphene flakes were fabricated by e-beam lithography using a typical bilayer resist (MMA/PMMA) and lift-off process. This step was performed first to prevent fine milled features by HIM on graphene samples from getting damaged during subsequent resist coating and/or lift-off. The prepared samples were then taken for HIM milling. To minimize beam-induced hydrocarbon deposition during patterning our graphene samples, the chamber was cleaned overnight, prior to the exposures with an integrated Evactron RF plasma cleaner. For milling graphene samples, the acceleration voltage and the beam current were adjusted to 30 kV and 1 pA, respectively. Thin graphene flakes were identified by secondary electron (SE) imaging at low magnifications. The He-ion beam was then carefully focused on a flake, using the corner/edge of the flake, at high magnification to ensure good focus of the beam for high resolution milling (see Fig. 2).

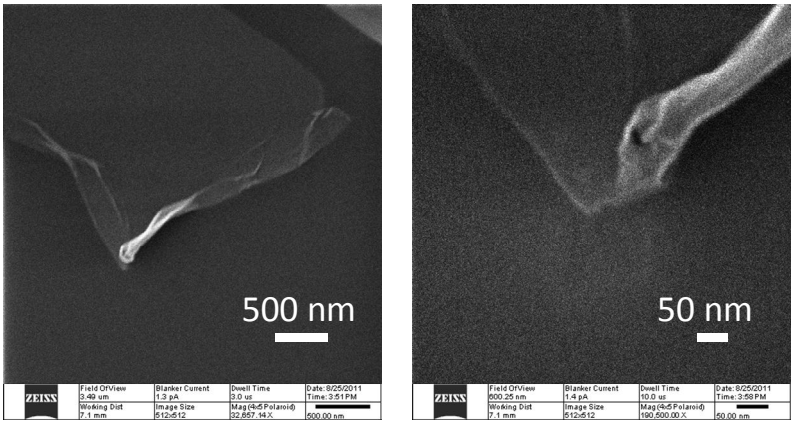

Figure 2 Image of a monolayer graphene flake taken by HIM. The scanning quality was maximized using the corner of the flake to ensure good milling results.

The magnification was then reduced, the flake was centred to the field of view, and the beam was blanked. Finally by using the Zeiss Orion UI software, the beam was scanned in the desired patterns to mill the graphene flakes. For our high resolution DQDs structures, we used a field of view of 700 nm × 700 nm for an image size of 512 × 512 pixels with ~ 1 nm pixel spacing. By altering dwell times, a range of doses between 0.3 and 0.7 nC/μm^2 were tested. However, initial exposures were not successful as seen in Fig. 3 which shows build-up rather than removal of material in the exposure area.

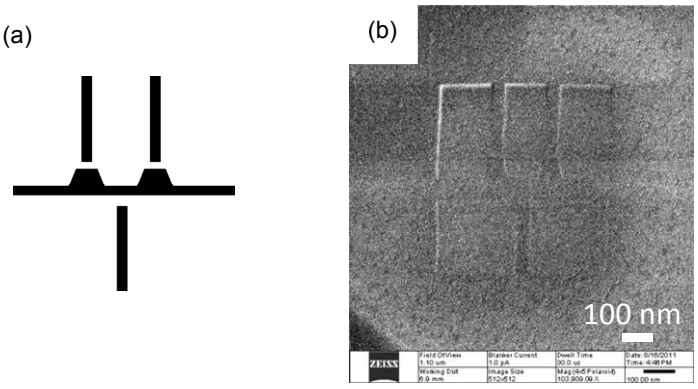

Figure 3 (a) The design of the milled pattern, (b) HIM secondary electron image of exposed monolayer graphene flake, showing build-up of contamination rather than successful milling.

These unsuccessful patterning results are in clear contrast to our early demonstration (Fig. 1(c)) which was conducted on pristine graphene flakes immediately after exfoliation. We therefore realized that the surface of the graphene flakes was most likely becoming contaminated during the process of fabricating the metal contacts as a result of exposure to resists and solvents. This contamination could be increasing the surface roughness of the flakes [17], and could be interacting with the helium ion beam to produce the deposits seen in Fig. 3(b). To clean our graphene flakes the samples were annealed at ≈330 °C with 1.3 L/min forming gas flow (6% H_2 and 94% N_2) for 1.5 hours. Remarkably, the milling results were significantly improved. For mono-layer (bi-layer) graphene flakes, a He dose of 0.6 nC/μm^2 (0.65 nC/μm^2) was chosen as the optimum dose for fabricating graphene devices. Figure 4 shows the result of successful milling on the very same flake shown in Fig. 3 after annealing.

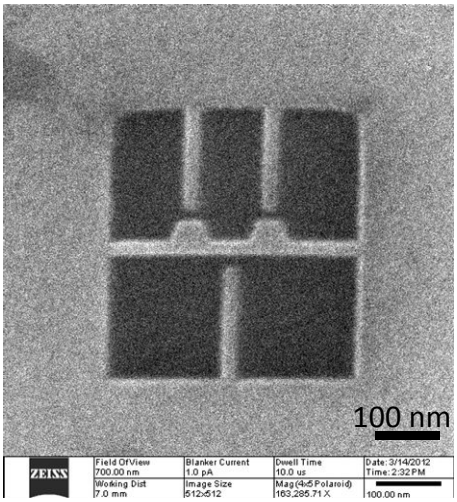

Figure 4 Successful milling after annealing the graphene sample. The milling was performed with an accelerating voltage of 30 kV, a beam current of 1 pA and a dose of 0.6 nC/μm^2. The distances between the side-gates and the QDs are ~ 10 nm.

We should mention that for fabricating a successful working graphene quantum dot (GQD)s device, one needs to fully isolate each side-gate. Due to limitations of the size of the patterns that can be imported into the Ziess Orion UI software, we have equipped our microscope with an XENOS external pattern generator which allows us to expose larger patterns. Examples of the structure of our GQDs/GDQDs are shown in Fig 5.

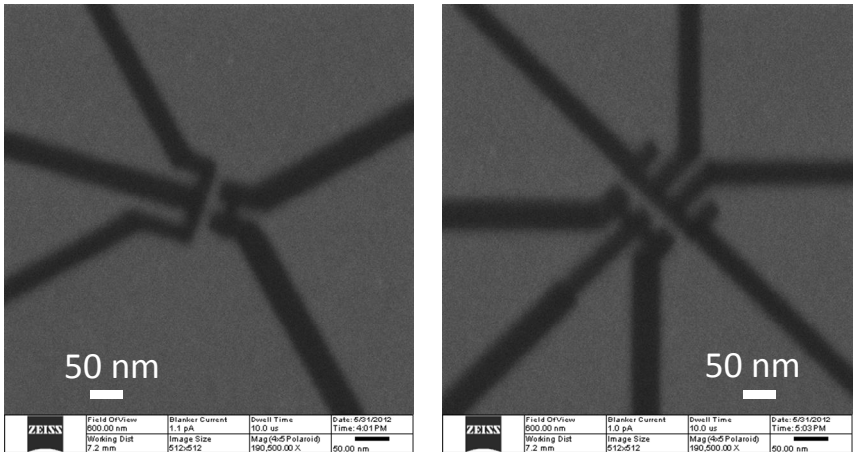

Figure 5 Examples of milled monolayer graphene flakes with GQDs and GDQDs patterns using XENOS external pattern generator.

Employing HIM has allowed us to pattern graphene flakes with very fine as well as symmetric patterns. This can be clearly seen in Fig 5 which shows 20 nm GQDs with ~ 15 nm wide gaps between the side gates and the QDs. The achieved dimensions and high fidelity are not possible using conventional e-beam lithography methods, especially in the case of graphene. For example, graphite pieces on the samples may hinder the uniform spinning of resist onto the samples which ultimately affects the resolution/size of the features in e-beam lithography. Moreover, ion scattering during RIE also limits the minimum size achievable with e-beam lithography.

3. IMPACTS OF HELIUM ION EXPOSURE ON CARREIR TRANSPORT IN BILAYER GNRS

In this section we present our recent study of the impacts of He ion exposure on carrier transport using electrical measurements of bilayer graphene (BLG) nanoribbons. Despite the large amount of literature regarding the scattering processes in single and bilayer graphene (SLG and BLG), disorder-induced scattering in BLG is not well understood. It is well known that in SLG, on silicon oxide substrates, the linear dependence of the conductivity on the charge density is attributed to charged impurities scattering i.e. $\sigma = ne\mu$ [18, 19]. In most situations, the charge impurity density is in the order of few 10^{11} cm^{-2}. In this case the mobility is constant and independent of n. Short range scattering in SLG introduces a sub-linear bending in the dependence of the conductivity at larger charge carrier densities [20]. The latter is attributed to vacancies and chemisorbed molecules or atoms which introduce the so-called mid-gap states. These particular defects are also called resonant scatterers as they strongly couple to graphene electronic states and thus scatter carriers very efficiently [21]. At low carrier density (close to the neutrality point), a minimum conductivity σ_{min} prevails caused by the random potential from charged impurities which breaks graphene into electrons and holes puddles. This minimum conductivity is related to a carrier characteristic density n* given by $\sigma_{min} = n^* e\mu$. The values of σ_{min} are on the order of a few e^2/h and the corresponding mobility is inversely proportional to the charged impurity density. The situation in BLG is quite different as the random potential from charged impurities is screened and at the NP the prevailing carrier density is a function of the puddle correlation length i.e. $n^* = \sqrt{n_{imp}/\xi^2}$. In BLG, both the screened Coulomb scattering and the short range scattering contribute linearly to the conductivity i.e. $\sigma \sim n$, whilst bare Coulomb screening contributes quadratically to the conductivity [22]. Several authors have investigated the role of midgap states introduced extrinsically into graphene or its bilayer by subjecting SLG or BLG to irradiation or doping with molecular species [23-26]. For example, Chen *et al*. [23] have shown that the mobility decreases as a consequence of midgap state scattering induced by increasing ion dosage. In reference [26] the effect of disorder in the Raman spectra of graphene subjected to low energy Ar+ ion bombardment was investigated, showing two length scales that characterize ion-induced lattice disorder and Raman scattering electron-relaxation length. Their method allowed the quantification of the density of defects and the average distance between defects in graphene.

Graphene nanoribbons (GNRs) of 2 um in length and 200 nm in width were defined using ebeam lithography and oxygen plasma etching. Prior to ebeam lithography an optical method confirmed the bilayer nature of the flakes where the nanoribbons are defined. To contact the GNRs, we used Ti and Au (5nm/95 nm) to define electrodes which were fabricated using ebeam lithography and a liftoff process. Prior to any electrical measurements, the nanoribbons were annealed at 350 ^{o}C for several hours.

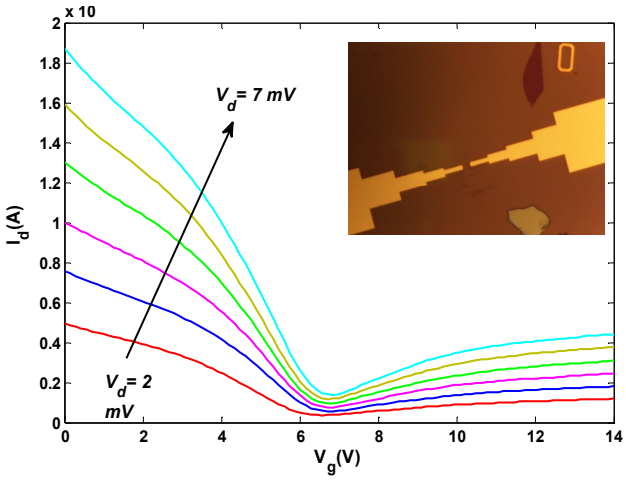

Figure 6 A set of Id-Vg characteristics of a graphene nanoribbon where the drain voltage was varied from 2 mV to 7 mV; Inset: one of the GNR samples, 2 um long and 200 nm wide used in the current experiment; also shown Ti/Au contact electrodes. The NGR is located between the two electrodes.

Irradiation with helium ions was performed at high vacuum in a helium ion microscope (HIM). The focused helium ion beam had a spot size of approximately 0.5 nm and was scanned over a square area centred on the graphene nanoribbon

location. Three different doses were used: 1.49×10^{13} ion/cm^2, 2.34×10^{13} ion/cm^2 and 4.16×10^{13} ion/cm^2. The maximum dose approximately equals to one He ion per 100 carbon atoms. Immediately prior to each irradiation run, the nanoribbons were annealed at 350^{o}C for several hours. Figure 6 shows a typical set of Id-Vg characteristics where the Dirac point (DP)is in the positive side of the gate voltage, indicating a residual doping of holes in the GNR channel. Even after several annealing runs, the purpose of which is to clean the nanoribbons of the resist residue, the DP was still positive. This hints to the possibility that the hole doping is not due to oxygen or water molecules adsorbed on the graphene surface, but to charge traps residing at the graphene/SiO_2 interface. This was confirmed by a persistent hysteresis in the resistance of the nanoribbons as shown in Fig. 7(a). In Fig. 7(b) we show the resistance of the GNR as a function of the radiation dose where an increase in the resistance as the dose increased is clearly visible. These curves were plotted as a function of V_g-V_{NP} for each radiation dose and for the pre-radiation state. There is no observable trend in the shift of the NP when the dose is increased in contrast to other experiments where a clear shift was observed when graphene was subjected to radiation.

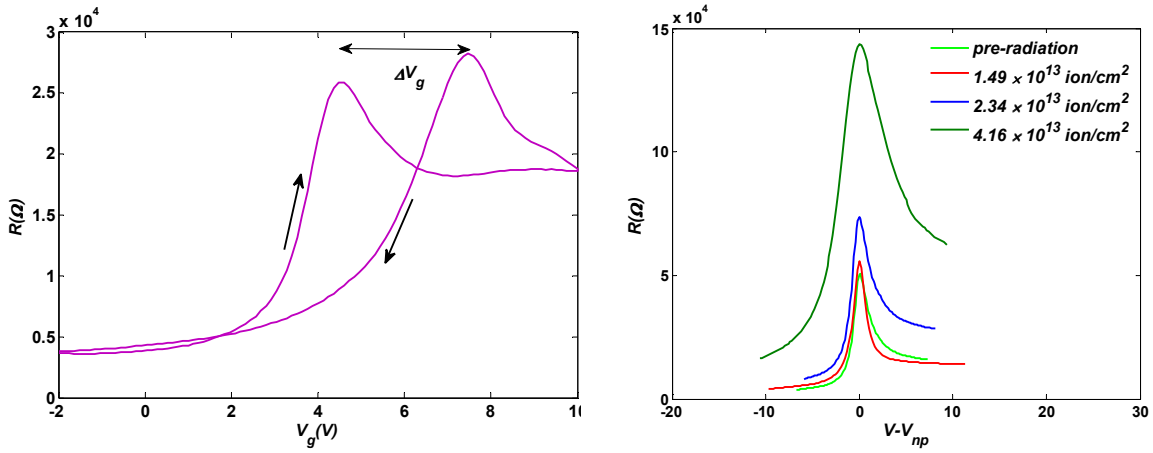

Figure 7 (a) Measured resistance of the graphene nanoribbons showing a hysteresis as the gate voltage is swept from left to right and back and (b) measured resistance of the GNR as function of the He ion dose. The resistance of the pre-radiation state is also shown (right).

Plotting the resistance as a function of V_g-V_{NP} gives a clearer picture of the scattering process as the impurities (or defects) are introduced into the graphene channel and the surrounding area. The resistivity of the GNRs can be estimated using $\rho = R\,w/L$, where R is the resistance (in Ω), w and L are the width and the length of the GNR respectively. To estimate the mobility we fit the relation, $\sigma^{-1} = \left[c_g\mu\left(V_g - V_{NP}\right) + \sigma_0\right]^{-1} + \rho_s$, to the data as shown in Fig. 8 for different values of the radiation dose as well as for the pre-radiation state. Also shown is, the fit of the data to the above expression for the conductivity. Here, ρ_s is a residual resistivity and σ_0 is a small residual conductivity. Table 1 shows the mobility as a function of the applied dose. It is clear the mobility decreases with increasing dose and that its values are lower than the pre-radiation state of the GNR.

Table 1 Values of the mobility as a function of the radiation dose. The values are derived from a nonlinear regression fit to the measured data (see text).

Dose (x 10^{13}) (cm $^{-2}$)	0 (pre-radiation)	1.49	2.34	4.16
Mobility (cm^2/V.s) (x10^4)	5.64	4.34	2.71	0.5161

The conductivity as shown in Fig. 8 is clearly a nonlinear function of the carrier density, exept for the dose of 4.16×10^{13} ion/cm^2. We performed an R-square procedure to test the goodness of fit of the data to the above expression. For the data corresponding to pre-radiation states and for the first two values of the dose (i.e. 1.49×10^{13} ion/cm^2, 2.34×10^{13}

ion/cm^2), the R-square value was approximately 99.6%. This value corresponding to the last applied dose (i.e. 4.16 × 10^{13} ion/cm^2) does not exceed 79%, however the linear fit puts this value up towards 99.6%. The He^+ irradiation decreases the minimum conductivity, decreases the mobility and suppresses the nonlinearity. The transition from nonlinear to linear behaviour is also clearly observed for positive values of the centred gate voltage (except for the last radiation dose). Our experimental data are in sharp contrast to the findings in references [27, 28]. In reference [28], experimental results for bilayer graphene show a clear linear dependence of the conductivity away from the NP and this is true for a wide range of temperatures. The result in reference [28] also shows that the conductivity is weakly dependent on temperature. In reference [27], the deposition of potassium on BLG made the dependence of the conductivity on the gate voltage nonlinear, in contrast to our present results where the He radiation induces a transition from nonlinear to linear behaviour, at least in the range of gate voltages shown (Fig. 8). As demonstrated in other experiments, our results for the pre-radiation state as well as for moderate He^+ doses, cannot be explained by bare Coulomb disorder where the conductivity is superlinear ($\sim n^2$) [22]. Neither can they be explained by screened Coulomb disorder nor short range disorder as this leads to a linear dependence of the conductivity on the carrier density [22]. Hence, we hypothesize that for the pre-radiation state of the GNR and moderate He+ irradiation, the scattering is mainly dominated by the edge disorder of the nanoribbons. The effect of the irradiation is to reduce the mean free path by introducing defects on the BLG and charged impurities in the surrounding areas.

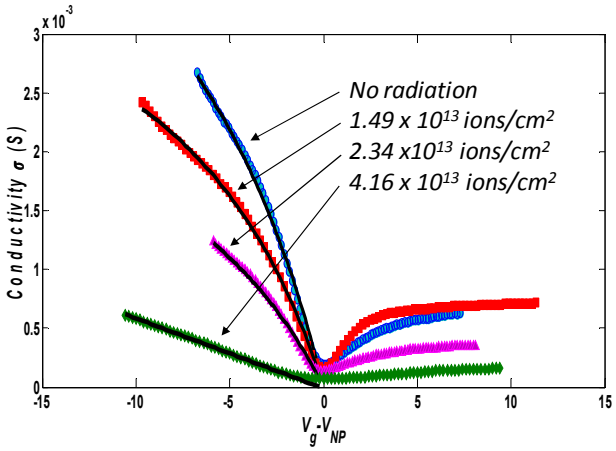

Figure 8 Conductivity of the GNR as a function of the centred gate voltage (or n-n_{NP}), for different applied He+ doses. The black lines are the fit to the data (see text). Blue circles correspond to the pre-radiation state; red squares, purple triangles and green diamonds correspond to doses of 1.49 × 10^{13}, 2.34 × 10^{13} and 4.16 × 10^{13} ion/cm^2, respectively.

We also conducted post-radiation Raman spectroscopy to study the damage caused by He ion bombardment [29]. Damage to the graphene lattice manifests in the emergence of the D peak at around 1350 cm^{-1} [23]–[26], and the ratio of this D peak to the G peak, present in pristine and damaged graphene at around 1605 cm^{-1} provides a measure of the extent to which the lattice is damaged. Figure 9(b) plots the average D to G ratios as a function of He ion dose which clearly shows the disorder induced by the He ions increases with the dose.

We performed Monte Carlo simulation [30] to investigate the penetration depth of He ions into a 300 nm oxide layer. The simulations show that He ions at the accelerating voltage of 30 kV used in our experiments penetrate deeper than 100 nm into the substrate oxide. The distribution of the He ions as a function of the oxide depth is shown in Fig. 10. It is clear that the tale of the distribution at the surface of the oxide (where graphene resides) accounts for less than 1% of the whole number of ions entered into the oxide layer. Therefore, we can comfortably say that the mobility degradation seen in our experiments is mainly due to defect-induced scattering and not the extra charged He^+ ions introduced in the specimen. At a large dose, the defect density is high enough so that the scattering is completely dominated by short range scatterers and hence the linear behaviour of the conductivity for a He ion dose of 4.16 × 10^{13} ion/cm^2.

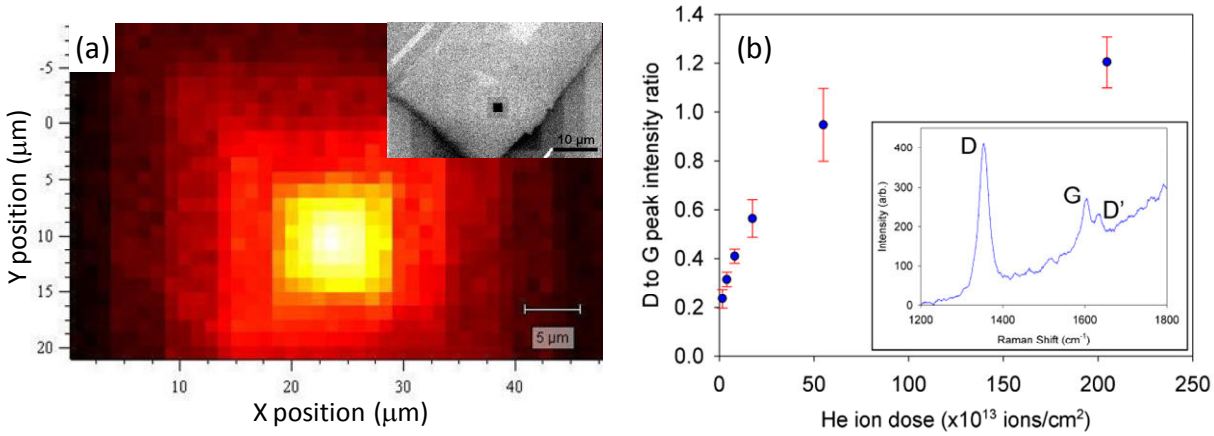

Fig. 9 D to G peak intensity versus dose for exposure of graphene monolayer to 30 kV He ion beam, the inset shows Raman spectrum for area exposed at a FOV of 5 µm..

To test our hypothesis we derive the mean free path (MFP) using the Drude-Boltazmann transport theory. Within this framework, the mean free path is given by the equation $2e^2/h(k_F l) = ne\mu$, where $k_F$is the Fermi wave vector and l the mean free path. For our experiments, the MFP derived for unbombarded nanoribbons is approximately $l \approx 208\,nm$ for a carrier density $n \approx 1 \times 10^{11} cm^{-2}$. This value is remarkably close to the width of our nanoribbons (200 nm) within the uncertainty of nanorribons width introduced during plasma etching of graphene. If we neglect phonon scattering in BLG compared to short range scattering, the value of the MFP $l \approx w$, w being the width of the GNR, in non-radiated GNR indicates that the scattering is limited by the disorder in the edges of the GNR (or line roughness). The MFP decreases with increasing dose and its values are $l = 164\,nm$, $l = 100\,nm$ and $l = 18\,nm$ for the applied doses of 1.49 x 10 ^{13} ion/cm^2, 2.34 x10^{13} ion/cm^2 and 4.16 x 10^{13} ion/cm^2 respectively. Hence the scattering is no longer limited by the edge disorder at high doses.

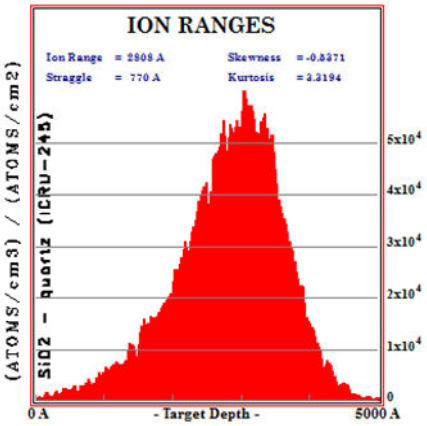

Figure 10 Distribution of helium ions calculated from a Monte Carlo simulation of helium ion bombardment of a 500 nm layer of SiO_2. The distribution is centred around a depth of 300 nm.

4. *AB-INITIO* STUDY OF CARRIER TRANSPORT IN DOWNSCALED GNRS WITH POINT DEFECTS

In this final section we present our recent attempts of studying the effects of disorder on the electronic states and carrier transport in downscaled GNRs by using the atomistic simulation. As discussed in the previous section, defects are created in the GNRs during He ion beam exposure. These defects strongly affect the electronic properties of the device. In addition, defects lead to rehybridization of sigma and pi orbitals which again has influence on the electronic structure of nanoribbons. In particular, point defects in graphene usually act as scattering centers for the incoming electron waves and also may give rise to dangling bonds which reduce the conductivity of the device [29].There are three major point

defects possible in the nanoconstriction-introduced region, namely single vacancy defects (SV), double vacancy defects (DV) and the Stone-Wales defects (SW).

Figure 11(a) shows the single-layer arm-chair GNR (AGNR) without defects. Single Vacancy defect refers to the condition where a single lattice atom is missing (Fig. 11(b)). Double Vacancy defect refers to the condition where two neighboring atoms are missing from the lattice. Here the atoms rearrange themselves to form a dangling bond-less structure as shown in Fig. 11(c) such that two five-edged polygons and one eight-edged polygon appear in the structure in place of four hexagons. This ability to reconstruct to form non hexagonal rings is one of the unique properties of graphene. Stone-Wales defect refers to the condition where four hexagons reconstruct to form two five-edged polygons and two seven-edged polygons as shown in Fig. 11(d). One of the C-C bonds undergoes a 90° twist. The number of atoms present is the same as that of the defectless junction and there is no dangling bond present. This defect may have been caused by an electron/ion impact or by an electron/ion beam that transfers energy less than the threshold required for knock on displacement.

For the present simulation, SIESTA [30], a DFT based ab initio simulation package for calculating the electronic states of the sample, is used. TranSIESTA [31], which solves the nonequlibrium Green's function theory in a self-consistent manner, is used for calculating the transport properties between nanoscale electrodes. The exchange-correlation is approximated by the Generalized Gradient Approximation (GGA). Hydrogen passivation has been done. The leads, made of graphene, were attached to the left and right side of this tunnel junction. In this simulation electrode width was kept two atomic distances larger than the AGNR region width. It should be mentioned that we adopt only the AGNR in the present study as the zig-zag GNRs (ZGNRs) do not generate a finite bandgap. It is obviously unrealistic to assume such perfect arm-chair edges as it is widely known from the STM studies that the edge states we have in reality with patterned or just exfoliated graphene are a mixture of zig-zag and arm-chair edge states. Our recent study [32], however, reveals that the arm-chair edge states locally generated in the ZGNRs with atomscale edge fluctuation results in the formation of a finite bandgap which is as wide as the one achieved with the AGNRs. Extension of the present defect analysis to the GNRs with the mixed edge states is left for future study.

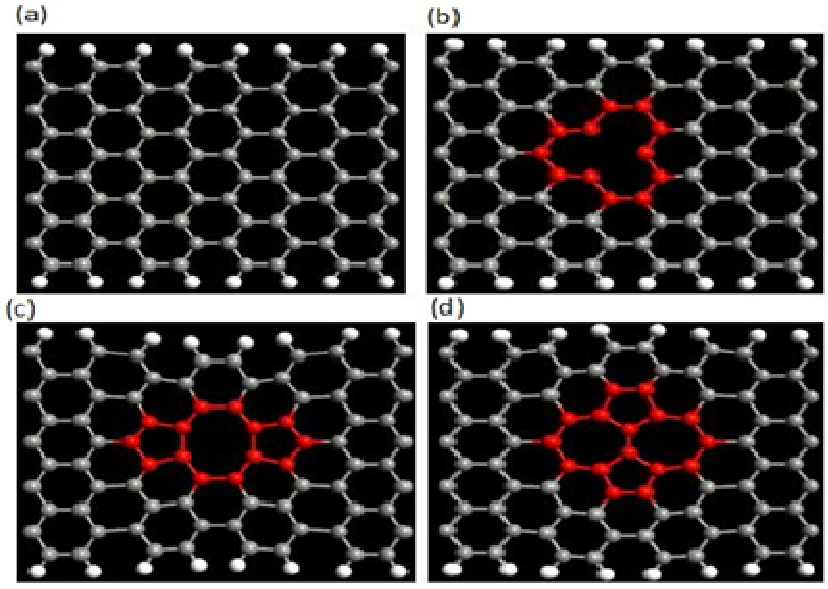

Figure 11 A single layer AGNR with (a) no defect, (b) a Single Vacancy defect, (c) a Double Vacancy defect, and (d) a Stone-Wales defect. The red bonds indicate the region of defect.

Figure 12(a) shows the transmission spectrum calcualted for the defectless AGNR under various values of potential bias. The stepwise nature seen in the transmission spectra under zero bias (a black solid line) reflects conductance quantization which is in common with one-dimensional quantum wires. As bias voltage increases, the entire transmission spectra shifts to lower energies, and the stepwise spectrum is gradually distorted with an appearance of a new broad peak at high

bias voltages since the electronic states within the lattice of the atoms are heavily affected by the applied bias. Figure 12(b) shows the transmission spectrum for the AGNR with a single vacancy defect. It is clear that the transmission coefficients decrease overall to lower than those for the defectless AGNR at a given energy and a given bias because of the presence of dangling bonds and resulting enhanced scattering. The broad peaks that emerge at high bias voltages are higher than those for defectless AGNR. This is attributed to the strong defect nature of the single vacancy [33].

Figure 13 shows the transmission spectra for the defectless, Double vacancy defect and stone-wales defect AGNRs. It can be clearly seen that the stepwise nature of the transmission spectra is heavily distorted for the AGNRs with the DV and SW defects. This signifies carrier scattering is enhanced due to restructuring of bonds which introduces large stress in the bonds. Neverthelss, the overall values of transmission coefficients for the AGNRs with the DV and SW defects are still close to that of the defectless AGNRs. This is expected as all carbon atoms in these samples have sp2 bonding and there is no dangling bonds as compared to the single vacancy nanoconstriction.

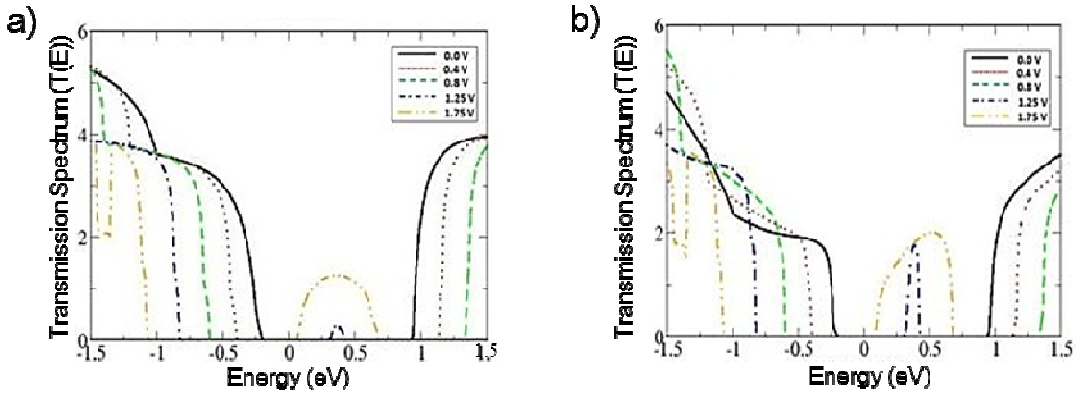

Figure 12 Transmission Spectrum of the AGNR (a) with no defect and (b) with single vacancy defect for various bias potentials.

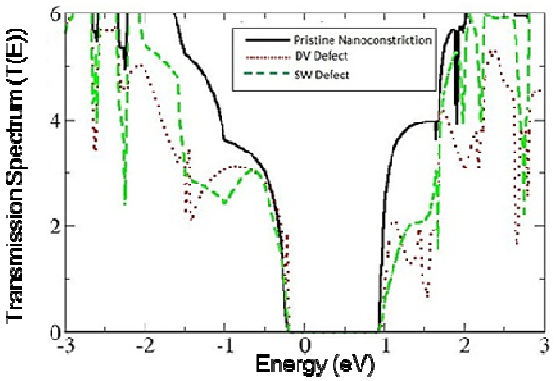

Figure 13 Transmission Spectra calculated for the AGNR with no defect and those with the DV and SW defects

5. CONCLUSION

We have described our new graphene nanofabrication approach based on direct milling of graphene using an atomic-size helium ion beam in the HIM. The helium ion beam milling process conducted after EB lithography was used to pattern metal contacts onto the graphene flakes. It was found that complete cleaning of the graphene surface is vital to remove the residue of EB resist and solvent which prevents successful milling. Double graphene QDs of 20 nm in dimensions and extremely narrow gaps down to 10 nm between the QDs and side gates were successfully achieved. Secondly we have investigated the effects of the helium ion exposure on the carrier transport properties by varying the helium ion dose onto the bilayer GNR transistor. The transfer characteristics measured at room temperature showed a remarkable decrease in

the conductivity by over 80% at a dose of 4.13×10^{13} ions/cm^2 which is approximately equivalent to one He ion per 100 carbon atoms. We also observed that the gate bias dependence of conductivity changes from nonlinear to linear with increasing dose, which implies GNR edge disorder can be a dominant carrier scattering mechanism. Finally we have studied the effects of three different types of defects, Single Vacancy defect, Double Vacancy and the Stone-Wales defect, introduced into extremely-scaled AGNRs on the carrier transport properties by using *ab initio* simulation.

REFERENCES

[1] Novoselov , K. S., Geim ,A. K., Morozov ,S. V., Jiang, D., Zhang , Y., Dubonos, S. V., Grigorieva, I. V. and Firsov , A. A., "Electric field effect in atomically thin carbon films", Science 306(5696),666-669 (2004).

[2] Geim , A. K. and Novoselov K. S., "The Rise of Graphene", Nature Materials 6, 183-191 (2007).

[3] Bolotin, K. I., Sikes, K. J., Jiang, Z., Klima, M., Fudenberg, G., Hone, J., Kim, P. and Stormer H. L., "Ultrahigh electron mobility in suspended graphene", Sol. Stat. Commun. 146(9-10), 351-355 (2008).

[4] Liao, L., Lin, Y. -C., Bao, M., Cheng, R., Bai, J., Liu, Y., Qu, Y., Wang, K.L., Huang, Y., Duan, X., "High-speed graphene transistors with a self-aligned nanowire gate", Nature 467(7313), 305 (2010).

[5] Schedin, F., Geim, A.k., Morozov, S.V., (2007). "Detection of individual gas molecules adsorbed on graphene". Nature Mater 6 (9), 652–655 (2007).

[6] Castro Neto, A. H., Guinea, F., Peres, N. M. R., Novoselov, K. S., and Geim, A. K., "The electronic properties of graphene", Rev.Mod.Phys , 81(1), 109-162 (2009).

[7] Goto, H., Kanda, A., Sato, T., Tanaka, S. Ootuka, Y., "Gate control of spin transport in multilayer graphene," Appl. Phys. Lett., 92(21), 212110 (2008).

[8] Chen, Z., Lin Y., Rooks, M. and Avouris, P., "Graphene nano-ribbon electronics", Physica E 40(2), 228-232 (2007).

[9] Stampfer, C., Güttinger, J., Molitor, F., Graf, D., Ihn, T. and Ensslin, K., "Tunable Coulomb blockade in nanostructured graphene", Appl. Phys. Lett. 92(1), 012102 (2008).

[10] Bell, D.C., Lemme, M. C., Stern, L. A., Williams, J. R. and Marcus, C. M., "Precision cutting and patterning of graphene with helium ions", Nanotechnology 20(45), 455301(2009).

[11] Pickard, D. and Scipioni, L., "Graphene Nano-Ribbon Patterning in the Orion Plus", Zeiss application note, Oct 2009.

[12] Ward, B. W., Notte, J. A. and Economou, N. P., Helium Ion Microscope: A new tool for nanoscale microscopy and metrology", J. Vac. Sci. Technol. B. 24(6), 2871-2874 (2006).

[13] Scipioni, L., Adv. Mater. Proc. 166 (2008) 27-30.

[14] Lemme, M. C., Bell, D. C., Williams, J. R., Stern, L. A., Baugher, B. W. H., Jarillo-Herrero, P. and Marcus, C. M., "Etching of graphene devices with a helium ion beam", ACS Nano 3(9), 2674-2676(2009).

[15] Boden, S. A, Moktadir Z., Bagnall D. M., Mizuta, H. and Rutt, H. N., "Focused helium ion beam milling and deposition", Mictroelectron. Eng., 88(8), 2452-2455 (2011).

[16] Lucchese, M. M., Stavale , Martins Ferreira, F., E. H., Vilani C., Moutinho, M. V. O., Capaz, R. B., Achete C. A. and Jorio A., "Quantifying ion-induced defects and Raman relaxation length in graphene" Carbon 48(5), 1592-1597 (2010).

[17] Ishigami, M., Chen, J., H., Cullen, W., G., Fuhrer, M., S., Williams, E., D., "Atomic structure of graphene on SiO2," Nano. Lett 7(6), 1643-1648 (2007).

[18] Hwang, E. H., Adam, S., Das Sarma, S., "Carrier Transport in Two-Dimensional Graphene Layers", Phys. Rev. Lett. 98(18), 186806 (2007).

[19] Chen, J. -H., Jiang, C., Adam, S., Fuhrer, M. S., Williams, E. D. and Ishigami, M., "Charged-impurity scattering in graphene", Nat. Phys.,4(5), 377 (2008).

[20] Stauber, T., Peres, N. and Guinea, F., "Electronic transport in graphene: A semiclassical approach including midgap states", Phys. Rev. B, 76(20), 205423 (2007).

[21] Wehling, T. O., Katsnelson, M. I. and Lichtenstein, A. I., "Adsorbates on graphene: Impurity states and electron scattering", Chem. Phys. Lett., 476(4-6), 125-134 (2009).

[22] Adam, S. and Sarma, D. S., "Boltzmann transport and residual conductivity in bilayer graphene", Phys. Rev. B 77(11), 115436 (2008).

[23] Chen , J. -H., Cullen, W. G., Jang, C., Fuhrer, M.S. and Williams, E. D., "Defect Scattering in Graphene", Phys. Rev. Lett., 102(23), 236805 (2009).

[24] Ni Z. H., Pnomarenko, L. A., Nair, R. R., Yang, R., Anissimova, S. Grigorieva, I. V., Schedin, F., Blake, P., Shen, Z.

X., Hill, E. H., Novoslev, K.S. and Geim, A. k., "On resonant scatterers as a factor limiting carrier mobility in graphene", Nano Lett. 10(10), 3868–3872 (2010).

[25] Hong, X., Cheng, S. –H, Herding, C., Zhu, J., "Colossal negative magnetoresistance in dilute fluorinated graphene", Phys. Rev. B, 83(8), 085410 (2011).

[26] Lucchese, M. M., Stavale, F., Martins Ferreira, E. H., Vilani, C., Moutinho, M. V. O., Capaz, Rodrigo B., Achete, C. A., Jorio, A., "Quantifyingion-induced defects and Raman relaxation length in graphene Carbon", 48(5), 1592–1597 (2010).

[27] Xiao, S., Chen, J.-H., Adam, S., Williams, E., and Fuhrer, M., "Charged impurity scattering in bilayer graphene," Phys. Rev. B, 82(4), 041406 (2010).

[28] Morozov, S.V., Novoselov, K. S., Katsnelson, M. I., Schedin, F., Elias, D. C., Jaszczak J. A. and A. K. Geim, "Giant intrinsic carrier mobilities in graphene and its bilayer," Phys. Rev. Lett, 100(1), 016602 (2008).

[29] Boden, S., Moktadir, Z., Bagnall, D., Rutt, H. and Mizuta, H. (2011) "Beam-induced damage to graphene in the helium ion microscope" In, Graphene 2011 Conference, Bilbao, Spain, 11 - 14 Apr 2011.

[30] "www.srim.org," [Online].

[31] Banhart, F., Kotakoski, J. and Krasheninnikov, A. V., "Structural defects in graphene", ACS Nano, 5(1), 26–41(2011).

[32] Ordejón, P., Artacho, E. and Soler, José M., "Self-consistent order-N density-functional calculations for very large systems", Phys. Rev. B, 53(16), R10441- R10444 (1996).

[33] Brandbyge, M., Mozos, J. L., Ordejón, P., Taylor, J. and Stokbro, K., "Density-functional method for nonequilibrium electron transport", Phys. Rev. B, 65(16), 165401(2002).

[34] Cuong, N. T., Mizuta H., Otsuka N. and Chi, D. H., 'Ab-initio calculations of electronic properties and quantum transport in U-shaped grapheme nanoribbons', 6th conference of the Asian Consortium on Computational Materials Science (ACCMS-6), Singapore, September (2011)

[35] Chen, J.-H.,Cullen, W. G, Jang, C., Fuhrer M. S., and Williams, E. D., "Defect Scattering in Graphene", Phys. Rev. Lett. 102(23), 236805 (2009).